Effect of Nd^{3+} Nanoparticles on Physical and Optical Properties of Glasses

Raghavendra M N[1,a], Ashwajeet J S[1,b], Manjunatha S O[2,c]

[1] *Department of Studies in Physics, Davangere University, Shivagangotri, Davanagere-577007, Karnataka, India.*
[2] *Department of Physics, B.M.S College of Engineering, Bangalore-560 019, Karnataka, India.*

[a] rag28mn@gmail.com
[b] ashphysics358@gmail.com
[c] manjusirigere2011@gmail.com

Abstract

Neodymium nanoparticle (Nd^{3+} NPs) incorporated $40B_2O_3$-(30-x)TeO_2-$15Y_2O_3$-$15Na_2O$-xNd_2O_3 glasses via melt quenching technique. The amorphous structure of these glasses was established by X-ray diffraction (XRD) studies. The glasses were examined for density measurements using Archimedes' technique with toluene as the immersion liquid and density was found in the range between 2.92 and 3.34 g/cm³. Optical band gaps were studied by UV-visible spectroscopy. The indirect bandgap was observed in the range of 3.70 to 4.17 eV. Whereas the refractive index varies from 2.14 to 2.23. The correlation and comparable patterns were seen in the optical bandgap values derived from the ASF and DASF approaches.

Keywords: Density, molar volume (Vm), UV Vis., ASF, DASF.
Received 22 January 2025; First Review 21 February 2025; Accepted 22 February 2025

*** Address of correspondence**
Ashwajeet J S
Department of Studies in Physics
Davangere University, Shivagangotri,
Davanagere, Karnataka, India

Email: ashphysics358@gmail.com

How to cite this article
Raghavendra M N, Ashwajeet J S, Manjunatha S O, Effect of Nd^{3+} Nanoparticles on Physical and Optical Properties of Glasses, J. Cond. Matt. 2024; 02 (02): 86-93.

Available from:
https://doi.org/10.61343/jcm.v2i02.111

Introduction

The intrinsic benefits of glasses over crystalline materials have led to their extensive use in the design of photonic and optoelectronic devices [1]. The optical characteristics of doped glass systems containing rare earth oxides have been thoroughly investigated. These characteristics may be used to sensors, display devices, lasers, fiber amplifiers, waveguide amplifiers for optical transmission networks, and telecommunications [2-3]. Optical devices can use borate glasses because they can dissolve rare-earth ions, are simple to make, and are clear even when exposed to UV light. Adding borate oxide to tellurite oxide also makes the glass more stable and of higher quality, makes it clearer, and makes it less hygroscopic [4]. The combination of TeO_2 and B_2O_3 is better than silicate and phosphate glasses in a number of ways. Borotellurite glasses are a beneficial compromise between the advantages and disadvantages of B_2O_3 and TeO_2 [5]. For solid-state lighting systems, trivalent neodymium (Nd^{3+}) containing activated glasses are a very intriguing rare-earth ion. The development of novel host glass materials can optimize the spectrum properties of RE ions [6]. The endurance & physical characteristics of borate glasses are enhanced by the addition of yttrium oxide [7]. Due to their special optical and structural characteristics, these tiny neodymium particles combined with glass are very beneficial in a wide range of intricate applications [8].

This work's primary objective is to fabricate and examine borotellurite glasses with Nd^{3+} nanoparticles incorporated. Our study included a thorough analysis of the optical and physical characteristics of new glasses of batch $40B_2O_3$-(30-x)TeO_2-$15Y_2O_3$-$15Na_2O$-xNd_2O_3. We have successfully synthesized glass samples to achieve this goal. Their density, molar volume (V_m), and oxygen packing density (OPD) were measured using the Archimedes technique. Physical characteristics of these specified glasses were computed in detail. The amorphous characteristics of the samples were validated using XRD analysis and their molecular composition and arrangement were elucidated by FTIR analysis. For all glasses, we conducted UV-visible measurements between 200 and 800 nm. Many research has adopted the Absorbance Spectrum Fitting (ASF) and Derivative Absorption Spectrum Fitting (DASF) in lieu of Tauc's technique, since the band gap may be determined only from absorbance values [9-12]. In the present work we

have compared thoroughly between Tauc's method with ASF and DASF methods.

Preparation and Characterization Details

Neodymium (III) oxide nanoparticles (NPs),(Nd_2O_3), Tellurium (IV) oxide, (TeO_4), Sodium Carbonate, (Na_2CO_3), Yttrium (III) oxide,(Y_2O_3), and Boric acid (H_3BO_3) of high purity chemical powders were used to synthesize the samples without additional purification. In an electric furnace, 15 g of material was combined with agate mortar, put in a silica crucible, and heated to 1200 °C for 60 minutes. A molten sample is poured onto the brass plate and then quenched using a different brass plate during the casting process. Thermal and mechanical stresses of sample were alleviated by subjecting the glasses to annealing at 600 °C for duration of 1 hour. After treatment, samples were labelled TN0, TN1, and TN2 repressively. This illustrates the changes in the composition of tellurite(T) and neodymium oxide(N) in the glasses formulated as $40B_2O_3$-(30-x)TeO_2-$15Y_2O_3$-$15Na_2O$-xNd_2O_3, with x values of 0, 4, and 8 mol % respectively.

TN glasses in powder state were investigated for their amorphous nature using XRD. A chemical component and structural investigation for current TN glasses was performed using FTIR. Spectral absorbance of synthesized glasses measured in the region of 400–1500 cm^{-1}. To determine the density Archimedes' principle was used employing Toluene as the immersing liquid. The fabricated TN glasses underwent UV-Vis absorption analysis throughout a wavelength range of 200 to 800 nm.

Results and discussion

X-ray Diffraction Studies:

The XRD spectra of TN glasses are presented in Fig. 1. All glass samples exhibited significant diffusion in their X-ray diffraction spectra at lower scattering angles.

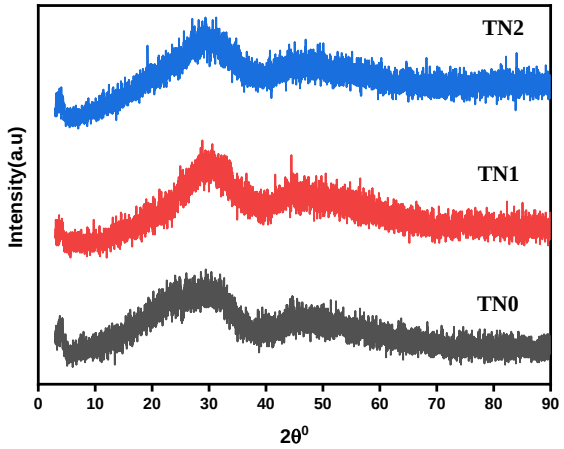

Figure 1: XRD pattern of the Nd^{3+} NPs TN glasses.

The pattern appears absence of sharp peaks and a broad and diffuse pattern between around 20^0-30^0 and 40^0-50^0, demonstrating that the glass samples are amorphous [8,13].

Fourier Transform Infrared (FTIR) Studies:

The FTIR spectra are shown in Fig. 2 over 400–1500 cm^{-1} range. The spectra include many peaks indicating local structure. Typical tellurite oxide structural units are about ~540 cm^{-1}. Tellurite oxide forms trigonal pyramidal (TeO_3) and trigonal bipyramidal (TeO_4) structures during glass production. The glass samples display a band representing the trigonal pyramidal TeO_3 structural unit at approximately 720 cm^{-1}.

Trigonal pyramidal TeO_3 in glass exhibit non-bridging oxygen atom distribution. Around 800 cm^{-1}, three spectral areas display a band group indicating the existence of bending vibrations caused by different combinations of borate. Tetrahedral BO_4 units' stretching vibrations are linked to the band group visible at around 1200 cm^{-1}. In trigonal BO_3 units, the elongation of B-O bonds leads to a distinct emphasis of the third band group at about 1400cm^{-1} [13-15].

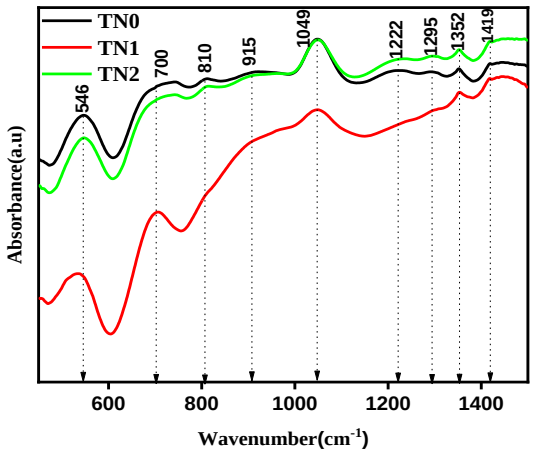

Figure 2: FTIR Absorption spectra of Nd^{3+} NPs TN glasses

Physical Studies:

The density of TN glasses was determined and subsequently calculated by following equation.

$$\rho = \frac{w_a}{w_a - w_t} \times \rho_t \qquad (1)$$

The glass's weight in air is represented by W_a, its weight in toluene by W_t, and its density in toluene (0.867 g/m^3) by ρ_t [16-17].

The following equation calculates molar volume (V_m) from density.

$$V_m = \frac{M_{glass}}{\rho_{glass}} \qquad (2)$$

Where M_{glass} represents average molecular weight of glass composition, while ρ_{glass} represents sample density [18]. The cation coordination number and oxide packing density (OPD). Its formula is:

$$OPD = 1000 \times \frac{N_o}{M_{glass}} \times \rho \qquad (3)$$

M_{glass} represents average molecular weight of glass, whereas N_o denotes number of oxygen atoms per oxide per unit formula [19]. The samples are viewed with excellent quality. The undoped Nd^{3+} glass sample exhibits the colourless and colour of the doped glass samples varies from light to bright purple, attributable to presence of Neodymium content. The Physical parameters of these glasses shown in Table 1 [20]. The association between each glass sample's density and molar volume and the Nd_2O_3 concentration (x wt%) is shown in Figure 3.

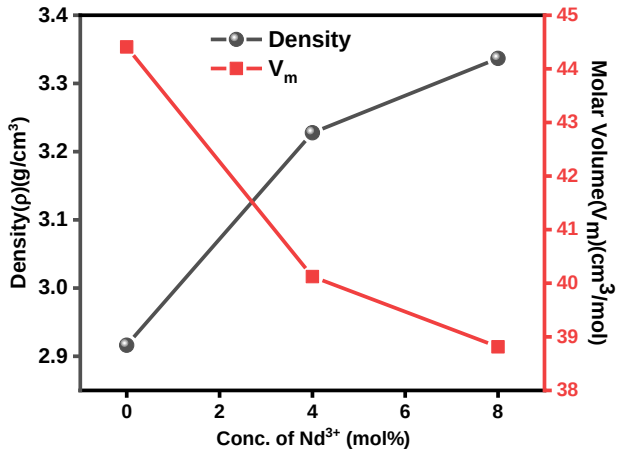

Figure 3: Density versus concentration of Nd^{3+} NPs with molar volume for TN glasses.

The association between each glass sample's density and molar volume and the Nd_2O_3 concentration (x wt%) is shown in Figure 3. The results of the experiment demonstrate that when the concentration of Nd_2O_3 in the samples increases, their density rises and molar volume decreases. The observed behaviour may be ascribed to disparity in molecular weights of TeO_2 (159.59 g/mol) and Nd_2O_3 (336.47 g/mol) reported in reference [21].

Table 1: Assessment of physical factors: density (ρ), molar volume (V_m), and oxygen packing density (OPD) of synthesized TN glasses.

Glasses	Nd^{3+} (%)	Physical parameters		
		Density (g/cm³)	V_m (cm³/mol)	OPD (g.atm/L)
TN0	0	2.916	44.408	54.04
TN1	4	3.228	40.124	60.80
TN2	8	3.337	38.814	63.89

Furthermore, Table 2 lists the physical parameters derived from the density data and refractive index. We analyse structural modifications in glass samples caused by variations in the concentration of Nd^{3+} NPs. The following physical characteristics of TN glasses are: The electrical dielectric constant, ionic concentration, inter-nuclear distance, molar polarizability, field strength, polaron radius, reflection loss, optical transmittance, metallization criterion, energy gap, optical basicity and dielectric constant of TN glasses were calculated using formulas found in the literature [22-23]. The findings presented in Table 2 show that doping of Nd^{3+} NPs cause a reduction in ionic concentration, polaron radius, molar polarizability, molar refraction inter-nuclear distance, they also enhance field strength, and optical basicity. electronic polarizability, dielectric constant, reflection loss, electronic susceptibility, and optical dielectric constant indicate an increase in TN1 and decrease in TN2 with an increase in Nd^{3+} NPs, Optical transmittance, metallization criteria, and energy gap indicate a drop in TN1 and rising in TN2 with a rise in Nd^{3+} NPs [24].

Table 2. Various physical factors of TN glasses

Sl. No	Physical property Parameters.	Glasses		
		TN0	TN1	TN2
		x=0	x=4	x=8
1.	Ionic concentration, N_i x10^{21} ion/cc	0	6.00	1.24
2.	Polaron Radius, r_px10^{-8} m	0	0.25	0.20
3.	Inter nuclear distance, r_i x10^{-8} m	0	0.63	0.5
4.	Field strength, F x 10^{15} cm^{-3}	0	46.54	73.88
5.	Molar refractivity, R_m cm^3/mol	28.93	26.67	24.87
6.	Electronic polarizability α_ex10^{-25} cm^3	2.20	2.26	2.15
7.	Molar polarizability α_m x10^{-24} cm^3	1.15	1.05	0.98
8.	Reflection losses, R_L(%)	0.14	0.15	0.13
9.	Optical Transmission, (T_o)	0.76	0.75	0.77
10.	Dielectric constant, ε	4.74	4.97	4.57
11.	Metallization criterion(M)	0.35	0.34	0.36
12.	Optical Basicity (^)	0.77	0.79	0.80
13.	Energy Gap (E_g)	2.43	2.25	2.58
14.	Electronic susceptibility, χ	0.30	0.32	0.28
15.	Optical Dielectric Constant, E_{opt}	3.74	3.97	3.57

UV-Vis. Studies:

Figure 4 displays the produced TN glasses' optical absorption spectra in the 300–800 nm region. The relative concentration of Nd_2O_3(x wt%) plays a significant role in determining the cutoff wavelength for each absorbance spectra. The picture shows eight absorption peaks, whereas the undoped glass sample TN0 has no peak. The peaks wavelengths of 353, 429, 469, 522, 584, 635, 683, and 746

nm are attributed. On the other hand, a shift in the absorption edges' positions causes the optical system's energy band gaps to vary. The origin of these phenomena is usually ascribed to the observed fluctuations in the concentration of Nd_2O_3.

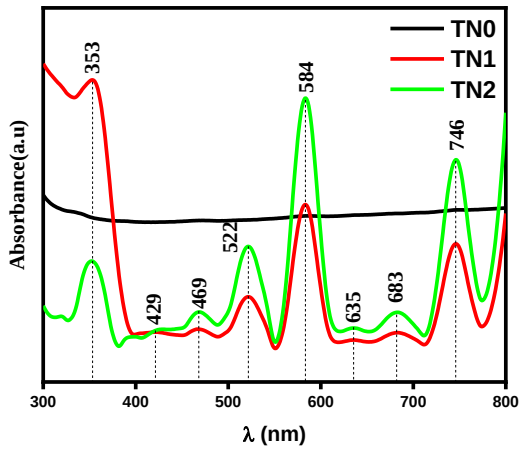

Figure 4: UV Absorption spectra of Nd^{3+} NPs TN glasses.

Band Gap of Optical Energy (E_{gap})

Tauc's model and the α(ν) optical absorption coefficient have been used to calculate energy gap for TN glasses [25]. Mott and Davis revised optical absorption coefficient α(ν) in Equation [25]. The power (r) is a precise measure of electronic transition characterised by a direct allowed transition at r = 0.5 and an indirect permissible transition at r = 2.0. For both direct and indirect allowed transition in suggested TN glasses, For both direct & indirect allowed transition in suggested TN glasses, Figure 5 and 6 illustrate the association of $(\alpha h\nu)^2$ and $(\alpha h\nu)^{0.5}$ in regard to (hν).

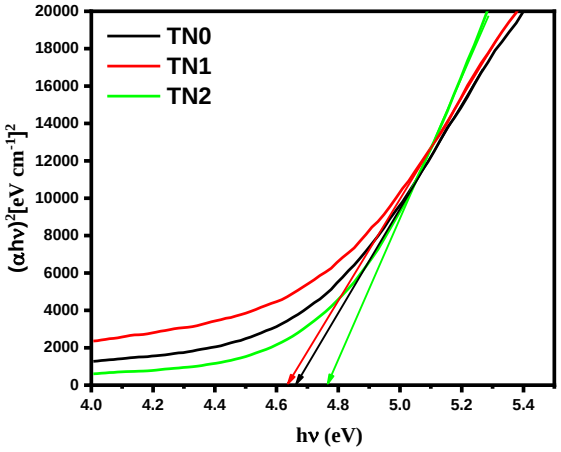

Figure 5: Variation of $(\alpha h\nu)^2$ versus (hν) for TN glasses.

To calculate values of $E_{g.dir}^{Tauc's}$ and $E_{g.indir}^{Tauc's}$ were extrapolated the straight line that passes over many points on the graphs at the locations where $(\alpha h\nu)^2 = 0$ and $(\alpha h\nu)^{0.5} = 0$, respectively. In Table 3, readings of $E_{g.dir}^{Tauc's}$ and $E_{g.indir}^{Tauc's}$ were provided. It was shown that the optical band gaps exhibited during direct transition had bigger diameters compared to those found during indirect transition. Moreover, it was observed that there was a considerable degree between the energy band gaps in each transition, indicating that the addition of Nd_2O_3 NPs to glass samples [26]. The indirect bandgap value spans from 3.709 to 4.174 eV. These results correspond with the optical gap values reported in [27]. The findings indicate that E_{opt} readings increases the indirect gap as concentration of Nd^{3+} nanoparticles rises from 0,4 & 8 mol%. Neodymium oxide ions' trivalent electrons change the absorbance properties via influencing the oxygen bonding in glass matrix [28]. The availability of loosely bound free electrons in respect to nuclear charge is increased by the presence of Nd_2O_3 ions, which aid in creation of NBOs. The valence and conduction bands are often excited by these free electrons, causing both bands to shift. The consequences of this change cause the forbidden gap to narrow, which lowers the reading of E_{opt} [29]. The indirect band gap value increases with the concentration of Nd_2O_3 owing to bonding defects.

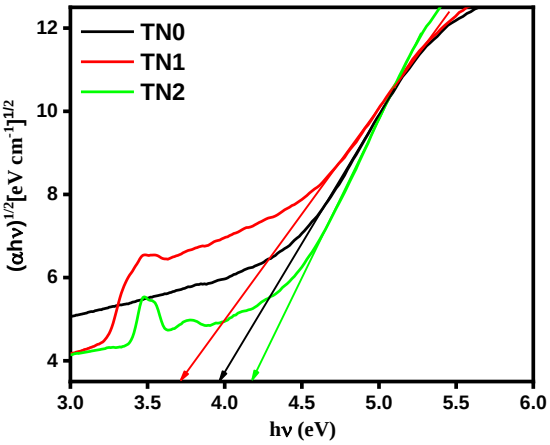

Figure 6: Variation of $(\alpha h\nu)^{1/2}$ versus (hν) for TN glasses

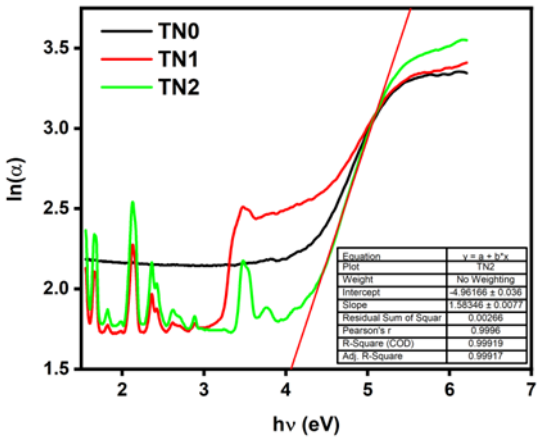

Figure 7: Variation of ln(α) versus (hν) for TN glasses

This alteration suggests subsequent introduction of Nd^{3+} ions into the glassy matrix modifies structural units and increases the amount of bridging oxygen, hence enhancing the magnitude of E_{opt}. Better connection within the glass network may potentially be the cause of an increase in E_{opt} readings. As more atoms bond, the separation between

valence and conduction bands expands, resulting in a rise in E_{opt} [30].

Under low photon energy conditions, the absorption coefficient (α) is governed by Urbach's empirical rule, as expressed in Eq. (4):

$$\alpha = \alpha_0 \exp\left(\frac{h\nu}{E_u}\right) \qquad (4)$$

where E_u and α_o stand for Urbach's energy and a constant, respectively. These values are often used to measure the size of the band tail originating from localized states within the band gap in low-crystalline or disordered materials. One may rephrase empirical Eq (4) as:

$$\ln\alpha = \ln\alpha_0 + \left(\frac{h\nu}{E_u}\right) \qquad (5)$$

Therefore, the Urbach's energy (E_u) determined by computing the gradient of the linear correlation between ln(α) & (hν). Fig. 7 depicts correlation between slope of linear function (α) and energy of photons (hν) for TN glasses, as shown in Table 3. The data suggest that glasses produced have the lowest Urbach's energy, suggesting the existence of very stable and consistent glasses with few flaws and a decrease in disorder within the glass samples that were made [31].

ASF Method, (E_g^{ASF})

Alarcon and associates have suggested a quantitative depiction of the α(ν) proportional to the photon wavelength (λ) [9] and Souri and Tahan [11]. The wavelength cutoff values for Planck's constant, light velocity and optical energy gap denoted as h, c, and λ_g respectively [32].

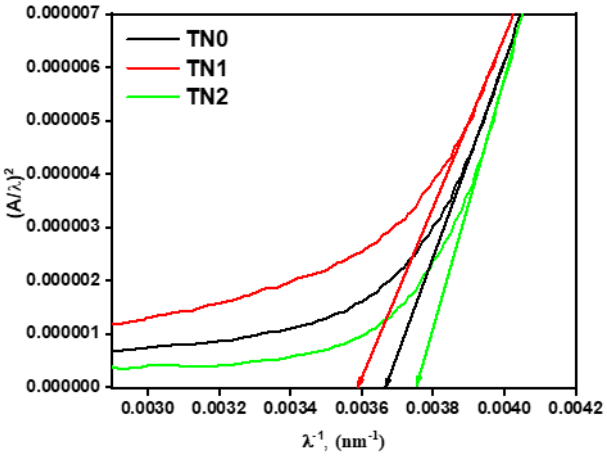

Figure 8: Change in $(A/\lambda)^2$ against λ^{-1} for TN glasses doped with Nd^{3+} NPs

The ASF approach, as indicated in Equation [25], facilitates determination of optical energy band gap only from absorbance measurements, disregarding thickness of glass sample. Additionally, optical gap within the ASF model may easily calculated using Equation (6) and calculating λ_g.

$$E_{gap}^{ASF} = \frac{hc}{\lambda_g} = 1239.83 \times \lambda_g^{-1} \qquad (6)$$

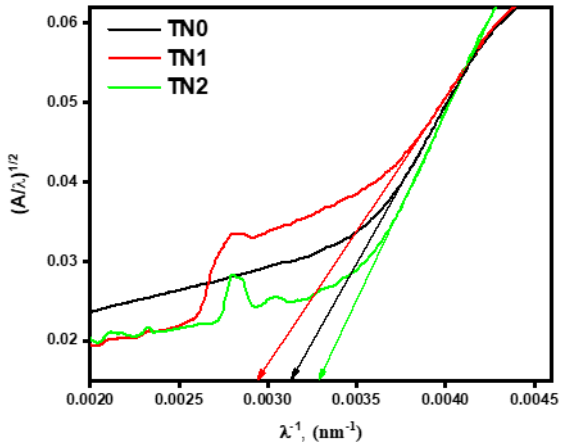

Figure 9: Change in $(A/\lambda)^2$ against λ^{-1} for TN glasses doped with Nd^{3+} NPs.

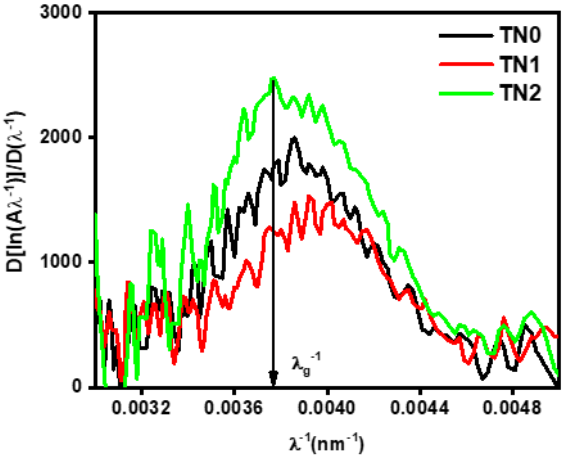

Figure 10: Graph of $d\{\ln[A\lambda^{-1}]\}/d(\lambda^{-1})$ against (λ^{-1}) for Nd^{3+} NPs doped in TN glasses. (DASF)

Figure 8 and 9 illustrate the variations in both direct and indirect transitions made possible by the proposed TN glasses [32]. Using extrapolation, the values of $E_{g.dir}^{ASF}$ and $E_{g.indir}^{ASF}$ were determined by identifying the straight area that passes over significant number of points on generated plots at points where $(A/\lambda)^2 = 0$ and $(A/\lambda)^{1/2} = 0$ respectively. In Table 3, the values of $E_{g.dir}^{ASF}$ and $E_{g.indir}^{ASF}$ are shown. Both Tauc's and ASF's approaches yielded very consistent outcomes [9].

DASF method, (E_g^{DASF})

The energy gaps of synthesised glasses were determined by DASF model. According to equation [22] where λ_g is the optical energy gap E_g^{DASF} calculate by

$$E_g^{DASF} = \frac{hc}{\lambda_g} = 1239.83 \times \lambda_g^{-1} \qquad (7)$$

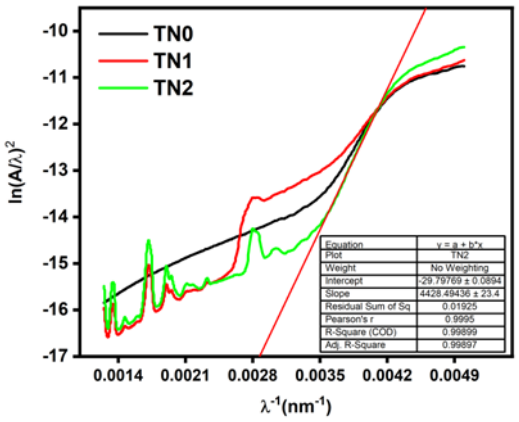

Figure 11: $DASF_{urb}$ plot of $\ln(A\lambda^{-1})^2$ vs λ^{-1} for TN glasses

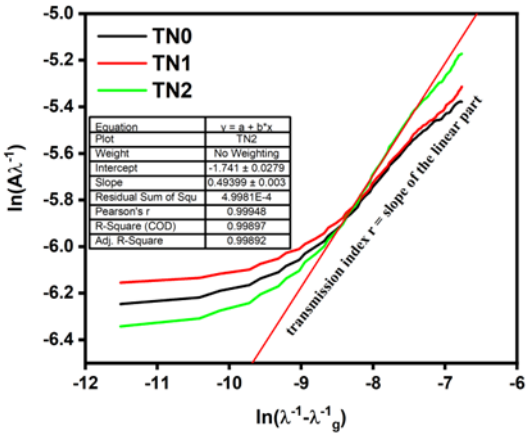

Figure 12: $\ln(A\lambda^{-1})$ versus $\ln(\lambda^{-1}\text{-}\lambda_g^{-1})$ plot for TN glasses doped with Nd^{3+} NPs. (transmission index: r)

Figure 10 illustrates the relationship between the derivative of TN glasses. The computed values of E_g^{DASF} were derived using Eq. (7) and reported in Table 3. The findings obtained from the evaluation of the three tests Tauc's, ASF, and DASF show a significant correlation with each other. Fig. 11 displays the dependence of $\ln(A\lambda^{-1})^2$ on λ^{-1} and shows the $DASF_{urb}$. The data show a strong correlation with Tauc's Urbach [33].The plot's linear section's slope, represented as $\ln((A(\lambda))/\lambda)$, may be compared to $\ln(1/\lambda - 1/\lambda_g)$ to get the r-value, as shown in the figure 12 [34].

This enables for the determination of the precise characteristics of the charge carrier optical transition. Table 3 lists 'r' as the slope of the fitted linear part. For all samples, it is about equal to 0.5, suggesting a direct transition. the calculation of refractive index factor (n) for all types of glasses. Through use of Eq. [18], We used Tauc's, ASF, and DASF techniques to compute the refractive index for permissible transitions that were both direct and indirect. The samples presented in Table 3 have their 'n' values derived from the current study. An inverse relationship was observed among the refractive indices and optical energy band gaps of analysed materials. Additionally, all of the glasses showed high n values, suggesting that they might be useful materials for optical and photoelectronic filter systems [32].

Table 3. Optical bandgaps (Tauc's, ASF, DASF), Refractive indices(n), Urbach energy (E_u) and Charge carrier optical transition (r) of present TN glasses.

Glasses		TN0	TN1	TN2	Ref
Tauc's	E_{dir}^{Tauc}	4.663	4.634	4.763	[35]
	n	2.053	2.056	2.037	-
	E_{indir}^{Tauc}	3.964	3.709	4.174	-
	n	2.177	2.229	2.137	-
	E_{urb}^{Tauc}	0.836	0.834	0.631	-
ASF	E_{dir}^{ASF}	4.493	4.447	4.649	-
	n	2.081	2.089	2.055	-
	E_{indir}^{ASF}	3.885	3.643	4.072	[36]
	n	2.192	2.243	2.156	[36]
DASF	E_g^{DASF}	4.773	4.860	4.661	-
	n	2.035	2.021	2.053	-
	E_{urb}^{DASF}	0.456	0.461	0.279	-
	r	0.4	0.4	0.5	-

Conclusion

This work primarily aims for examine the physical and optical characteristics of borotellurite glasses containing Nd^{3+} nanoparticles. The outcomes of the study highlight several significant characteristics of the TN glasses. XRD study verified the amorphous properties, whilst FTIR examinations elucidated molecular composition and structure of the glasses. The glass density analysis showed a rise from 2.92 to 3.34 gm/cm³, a decline in molar volume (V_m) from 44.40 to 38.81 cm³/mol, and rise in oxygen packing density (OPD) from 54.04 to 63.89 gm/cm³. Using Tauc's approach, indirect energy band gap vary between 3.71 eV & 4.17 eV, while the ASF and DASF methods showed variations from 3.64 eV to 4.07 eV & 4.66 eV to 4.86 eV, respectively. The slope of the fitted linear segment, 'r,' was almost 0.5 for every sample, suggesting a direct transition. Additionally, refractive index of TN1 glass was determined to be around 2.23, underscoring the potential of these glasses as efficient materials for photoelectronic applications and optical filter devices.

Acknowledgments

Authors sincerely acknowledge the UGC-DAE-CSR, Kolkata, for their provision of characterization facilities.

References

1. K. Siva Rama Krishna Reddy et al., *'Structural, optical absorption and photoluminescence spectral studies of Sm^{3+} ions in Alkaline-Earth Boro Tellurite glasses'*, Opt. Mater. (Amst)., vol. 79, pp. 21–32, 2018, doi: 10.1016/j.optmat.2018.03.005.
2. O. Ravi, C. M. Reddy, B. S. Reddy, and B. D. P. Raju, *'Judd–Ofelt analysis and spectral properties of Dy^{3+} ions doped niobium containing tellurium calcium zinc borate glasses'*, Opt. Commun., vol. 312, pp. 263–268, 2014.
3. Z. A. S. Mahraz, M. R. Sahar, S. K. Ghoshal, M. R. Dousti, and R. J. Amjad, *'Silver nanoparticles enhanced luminescence of Er^{3+} ions in boro-tellurite glasses'*, Mater. Lett., vol. 112, pp. 136–138, 2013.
4. A. Jha et al., *'Rare-earth ion doped TeO_2 and GeO_2 glasses as laser materials'*, Prog. Mater. Sci., vol. 57, no. 8, pp. 1426–1491, 2012.
5. J. S. Alzahrani, M. A. Alothman, C. Eke, H. Al-Ghamdi, D. A. Aloraini, and M. S. Al-Buriahi, *'Simulating the radiation shielding properties of TeO_2–Na_2O–TiO glass system using PHITS Monte Carlo code'*, Comput. Mater. Sci., vol. 196, p. 110566, 2021.
6. D. Ramachari, L. Rama Moorthy, and C. K. Jayasankar, *'Optical absorption and emission properties of $Nd3^+$-doped oxyfluorosilicate glasses for solid state lasers'*, Infrared Phys. Technol., vol. 67, pp. 555–559, 2014, doi: 10.1016/j.infrared.2014.09.020.
7. M. R. S. Nasuha, H. Azhan, W. A. W. Razali, L. Hasnimulyati, and Y. Norihan, *'Effect of yttrium on the physical, elastic, and structural properties of neodymium-doped lead borotellurite glass'*, J. Mater. Sci. Mater. Electron., vol. 32, no. 18, pp. 22890–22897, 2021, doi: 10.1007/s10854-021-06766-w.
8. M. N. Azlan and M. K. Halimah, *'Role of Nd^{3+} nanoparticles on enhanced optical efficiency in borotellurite glass for optical fiber'*, Results Phys., vol. 11, no. August, pp. 58–64, 2018, doi: 10.1016/j.rinp.2018.08.017.
9. L. Escobar-Alarcón, A. Arrieta, E. Camps, S. Muhl, S. Rodil, and E. Vigueras-Santiago, *'An alternative procedure for the determination of the optical band gap and thickness of amorphous carbon nitride thin films'*, Appl. Surf. Sci., vol. 254, no. 1 SPEC. ISS., pp. 412-415, 2007, doi: 10.1016/ j.apsusc.2007.07.052.
10. D. Souri and K. Shomalian, *'Band gap determination by absorption spectrum fitting method (ASF) and structural properties of different compositions of $(60-x)V_2O_5.40TeO_{2-x}Sb_2O_3$ glasses'*, J. Non. Cryst. Solids, vol. 355, no. 31–33, pp. 1597–1601, 2009, doi: 10.1016/j.jnoncrysol.2009.06.003.
11. D. Souri and Z. E. Tahan, *'A new method for the determination of optical band gap and the nature of optical transitions in semiconductors'*, Appl. Phys. B, vol. 119, no. 2, pp. 273–279, 2015.
12. A. A. Ali, Y. S. Rammah, R. El-Mallawany, and D. Souri, *'FTIR and UV spectra of pentaternary borate glasses'*, Meas. J. Int. Meas. Confed., vol. 105, no. April, pp. 72–77, 2017, doi: 10.1016/j.measurement.2017.04.010.
13. T. Walia and K. Singh, *'Mixed alkaline earth modifiers effect on thermal, optical and structural properties of SrO-BaO-SiO2-B2O3-ZrO2 glass sealants'*, J. Non. Cryst. Solids, vol. 564, no. April, p. 120812, 2021, doi: 10.1016/j.jnoncrysol.2021.120812.
14. A. Dehelean, S. Rada, A. Popa, and E. Culea, *'Structural and magnetic investigations on gadolinium–tellurite vitreous systems prepared by sol–gel method'*, J. Mol. Struct., vol. 1036, pp. 203–208, 2013.
15. S. K. J. Al-Ani, S. S. Al-Rawi, A. H. Jassim, and H. A. Al-Hilli, *'FTIR spectra of molybdenum tellurite glasses'*, Iraqi J. Appl. Phys, vol. 2, no. 1–2, pp. 23–25, 2006.
16. A. Madhu, B. Eraiah, P. Manasa, and N. Srinatha, *'Nd^{3+}-doped lanthanum lead boro-tellurite glass for lasing and amplification applications'*, Opt. Mater. (Amst)., vol. 75, pp. 357–366, 2018, doi: 10.1016/j.optmat.2017.10.037.
17. J. S. Ashwajeet, T. Sankarappa, T. Sujatha, and R. Ramanna, *'Thermal and electrical properties of $(B_2O_3$-TeO_2-Li_2O-CoO) glasses'*, J. Non. Cryst. Solids, vol. 486, pp. 52–57, 2018.
18. D. Saritha, M. Salagram, and G. Bhikshamaiah, *'Physical and optical properties of Bi_2O_3-B_2O_3 glasses'*, in IOP Conference Series: Materials Science and Engineering, IOP Publishing, 2009, p. 12057.
19. N. Yahya et al., *'Effect of silver on the physical and structural properties of lead neodymium borotellurite glass system'*, Malaysian J. Anal. Sci., vol. 22, no. 2, pp. 296–302, 2018.
20. M. R. S. Nasuha, H. Azhan, W. A. W. Razali, L. Hasnimulyati, and Y. Norihan, *'Structural and elastic properties studies of yttrium lead borotellurite glass doped with neodymium oxide'*, vol. 18, no. 8, pp. 439–448, 2021.
21. A. Kaur, A. Khanna, and L. I. Aleksandrov, *'Structural, thermal, optical and photo-luminescent properties of barium tellurite glasses doped with rare-earth ions'*, J. Non. Cryst. Solids, vol. 476, no. August, pp. 67–74, 2017, doi: 10.1016/j.jnoncrysol.2017.09.025.
22. N. J. Kreidl, *'Variability of optical properties and*

structure of glass', Glas. Berichte, vol. 62, no. 6, pp. 213–218, 1989.

23. J. A. Duffy, *'The electronic polarisability of oxygen in glass and the effect of composition'*, J. Non. Cryst. Solids, vol. 297, no. 2–3, pp. 275–284, 2002.
24. A. S. Rao, Y. N. Ahammed, R. R. Reddy, and T. V. R. Rao, *'Spectroscopic studies of Nd^{3+}-doped alkali fluoroborophosphate glasses'*, Opt. Mater. (Amst)., vol. 10, no. 4, pp. 245–252, 1998, doi: 10.1016/S0925-3467(97)00055-4.
25. A. S. Rao et al., *'Spectroscopic and optical properties of Nd^{3+} doped fluorine containing alkali and alkaline earth zinc-aluminophosphate optical glasses'*, Phys. B Condens. Matter, vol. 404, no. 20, pp. 3717–3721, 2009.
26. V. B. Sreedhar, R. Doddoji, K. K. Kumar, and V. R. M. Reddy, *'A study of NIR emission and associated spectroscopic properties of Nd^{3+}: $P_2O_5^+$ K_2O^+ $Al_2O_3^+$ ZnF_2 glasses for 1.06 μm laser applications'*, J. Non. Cryst. Solids, vol. 553, p. 120521, 2021.
27. S. Rani, N. Ahlawat, R. Parmar, S. Dhankhar, and R. S. Kundu, *'Role of lithium ions on the physical, structural and optical properties of zinc boro tellurite glasses'*, Indian J. Phys., vol. 92, pp. 901–909, 2018.
28. M. N. Azlan, M. K. Halimah, S. Z. Shafinas, and W. M. Daud, *'Electronic polarizability of zinc borotellurite glass system containing erbium nanoparticles'*, Mater. Express, vol. 5, no. 3, pp. 211–218, 2015.
29. M. N. Azlan, M. K. Halimah, A. B. Suriani, Y. Azlina, and R. El-Mallawany, *'Electronic polarizability and third-order nonlinearity of Nd^{3+} doped borotellurite glass for potential optical fiber'*, Mater. Chem. Phys., vol. 236, p. 121812, 2019.
30. M. R. S. Nasuha, H. Azhan, L. Hasnimulyati, W. A. W. Razali, and Y. Norihan, *'Effect of Nd3+ ions on Physical and Optical Properties of Yttrium Lead Borotellurite Glass System'*, J. Non. Cryst. Solids, vol. 551, no. August 2020, p. 120463, 2021, doi: 10.1016/j.jnoncrysol.2020.120463.
31. M. K. Halimah, A. A. Awshah, A. M. Hamza, K. T. Chan, S. A. Umar, and S. H. Alazoumi, *'Effect of neodymium nanoparticles on optical properties of zinc tellurite glass system'*, J. Mater. Sci. Mater. Electron., vol. 31, pp. 3785–3794, 2020.
32. Y. S. Rammah, K. A. Mahmoud, M. I. Sayyed, F. I. El-Agawany, and R. El-Mallawany, *'Novel vanadyl lead-phosphate glasses: P_2O_5-PbO-ZnONa_2O-V_2O_5: Synthesis, optical, physical and gamma photon attenuation properties'*, J. Non. Cryst. Solids, vol. 534, no. December 2019, p. 119944, 2020, doi: 10.1016/j.jnoncrysol.2020.119944.
33. D. Souri, M. Sarfehjou, and A. R. Khezripour, *'The effect of ambient temperature on the optical properties and crystalline quality of ZnSe and ZnSe:Cu NCs grown by rapid microwave irradiation'*, J. Mater. Sci. Mater. Electron., vol. 29, no. 4, pp. 3411–3422, 2018, doi: 10.1007/s10854-017-8276-5.
34. D. Souri, A. R. Khezripour, M. Molaei, and M. Karimipour, *'ZnSe and copper-doped ZnSe nanocrystals (NCs): Optical absorbance and precise determination of energy band gap beside their exact optical transition type and Urbach energy'*, Curr. Appl. Phys., vol. 17, no. 1, pp. 41–46, 2017, doi: 10.1016/j.cap.2016.10.008.
35. Y. A. Yamusa, R. Hussin, W. N. W. Shamsuri, Y. A. Tanko, and S. A. Jupri, *'Impact of Eu^{3+} on the luminescent, physical and optical properties of $BaSO_4$–B_2O_3–P_2O_5 glasses'*, Optik (Stuttg)., vol. 164, pp. 324–334, 2018.
36. I. Bulus, R. Hussin, S. K. Ghoshal, A. R. Tamuri, I. M. Danmallam, and Y. A. Yamusa, *'Europium-doped boro – telluro - dolomite glasses for red laser applications: Basic insight into spectroscopic traits'*, J. Non. Cryst. Solids, vol. 534, no. September 2019, p. 119949, 2020, doi: 10.1016/j.jnoncrysol.2020.119949.